PAPER

Check for updates

Efficient solar light-driven hydrogen generation using an Sn₃O₄ nanoflake/graphene nanoheterostructure†

Yogesh A. Sethi,[a] Aniruddha K. Kulkarni,[b] Anuradha A. Ambalkar,[a] Rajendra P. Panmand, [ID][a] Milind V. Kulkarni,[a] Suresh W. Gosavi*[c] and Bharat B. Kale [ID] *[a]

Herein, we report Sn₃O₄ and Sn₃O₄ nanoflake/graphene for photocatalytic hydrogen generation from H₂O and H₂S under natural "sunlight" irradiation. The Sn₃O₄/graphene composites were prepared by a simple hydrothermal method at relatively low temperatures (150 °C). The incorporation of graphene in Sn₃O₄ exhibits remarkable improvement in solar light absorption, with improved photoinduced charge separation due to formation of the heterostructure. The highest photocatalytic hydrogen production rate for the Sn₃O₄/graphene nanoheterostructure was observed as 4687 μmol h⁻¹ g⁻¹ from H₂O and 7887 μmol h⁻¹ g⁻¹ from H₂S under natural sunlight. The observed hydrogen evolution is much higher than that for pure Sn₃O₄ (5.7 times that from H₂O, and 2.2 times from H₂S). The improved photocatalytic activity is due to the presence of graphene, which acts as an electron collector and transporter in the heterostructure. More significantly, the Sn₃O₄ nanoflakes are uniformly and parallel grown on the graphene surface, which accelerates the fast transport of electrons due to the short diffusion distance. Such a unique morphology for the Sn₃O₄ along with the graphene provides more adsorption sites, which are effective for photocatalytic reactions under solar light. This work suggests an effective strategy towards designing the surfaces of various oxides with graphene nanoheterostructures for high performance of energy-conversion devices.

1. Introduction

Sunlight absorption and the ability to tune the optical band gap of materials is considered a plausible means to convert solar energy into fuel. The sunlight-driven production of hydrogen from water and H₂S occurs by breaking of a chemical bond, which is similar to what occurs in the natural photosynthesis process. The solar to chemical energy conversion (hydrogen evolution reaction (HER): $2H^+ + 2e^- \rightarrow H_2$), requires a large positive Gibb's free energy, $\Delta G = 237$ kJ mol⁻¹ for H₂O splitting, whereas H₂S splitting requires a free energy of $\Delta G = 33$ kJ mol⁻¹. Thus less energy is required for H₂S splitting.

Semiconductors with a narrow band gap have the potential to absorb maximum solar light.[1,2] However, the requirements of a functional photocatalytic system mean that the semiconductors must satisfy multiscale integrated approaches, wherein the catalyst should have enhanced solar light absorption capability, effective band edge position, efficient charge separation of electron–hole pairs, excellent chemical stability, low overpotential for water reduction, *etc.*

The first report using TiO₂ for electrochemical hydrogen generation from water was by Fujishima and Honda in 1970.[3] Similar to TiO₂, extensive research has been conducted to develop efficient photocatalysts for the HER, such as Nb₂O₅,[4] Fe₂O₃,[5] WO₃,[6] ZnO,[7] *etc.* However, the photocatalytic efficiency of these semiconductors was not adequate for industrial goals due to their high resistance, inappropriate band gap, and rapid charge carrier recombination rate.

In the past few decades a strategy has been developed to extend the absorption onset of pure TiO₂ towards longer wavelengths. This includes oxynitrides and the addition of noble metal nanoparticles on passive oxide semiconductors (Pt, Au, Ag, *etc.*). Further, the multiphoton excitation method, using heterojunction formation by combining two low band gap semiconductors, is used to enhance photocatalytic activity, as the photogenerated electrons can be scavenged, which ultimately increases the electron–hole separation efficiency.[8–10] Recently, the nonstoichiometric n-type Sn₃O₄ has been

[a]Nanocrystalline Laboratory, Centre for Material for Electronic Technology (CMET), Department of Information Technology, Govt. of India, Panchawati, Off Pashan Road, Pune 411007, India. E-mail: bbkale1@gmail.com; bbkale@cmet.gov.in; Fax: +91 20 2589 8180; Tel: +91 20 2589 9273

[b]Prof. John Barnabas School for Biological Studies, Department of Chemistry, Ahmednagar College, Ahmednagar 414001, India

[c]Department of Physics, Savitribai Phule Pune University, Pune 411008, India

† Electronic supplementary information (ESI) available. See DOI: 10.1039/d1ra05617d

considered as an attractive semiconductor due to its unique band gap and band edge potential.

Currently, global fossil fuel consumption drives strong growth in energy demand from modern civilization worldwide, posing serious challenges for the scientific community in the 21st century.[11,12] Among all the potential solutions being considered, splitting hydrogen (H_2) from H_2O and H_2S using solar light is one of the promising candidates for green energy, owing to the large energy density, nonpolluting nature, low cost, and low carbon emission.[13–15] Hydrogen sulfide (H_2S) is a toxic gas produced in large quantities from natural gas and oil refineries, hot springs, *etc*. The concentration of H_2S from natural gas increases daily in the atmosphere (8.6%), which seriously affects oxygen utilization and central nervous systems.[4] In this context, a semiconductor is used as an active photocatalyst for H_2 generation from splitting water and H_2S under sunlight.[16,17] In the past, semiconductor-based photocatalysts have been intensively studied due to their excellent stability under solar-active photocatalysts, and also examined as attractive candidates for water purification under solar light.[18] The major inherent drawback of Sn_3O_4 is its rapid charge carrier recombination rate under solar light.[19] Constructing heterostructures between Sn_3O_4 and other semiconductors, with appropriate positioning of conductance and valence bands, is an effective strategy to reduce the charge carrier recombination rate.[20]

Over the last few years, two-dimensional (2D) graphene has received much attention owing to its 2D, ultra-thin thickness, and some unusual physicochemical and optoelectronic properties compared with bulk materials. Graphene is a flat monolayer of sp^2 carbon atoms strongly packed into a 2D honeycomb lattice. Formation of a heterostructure of a metal oxide semiconductor with graphene is a promising approach to reduce the electron–hole pair recombination rate and increase the number of active sites for photocatalytic reactions.[21–23]

Two-dimensional graphene has a large surface area, good flexibility, and excellent electrical conductivity, which captures electrons and reduces charge carrier recombination. The attractive features of graphene provide stability to Sn_3O_4, which enhances hydrogen generation. Recently, Yu *et al.*, have demonstrated the solvothermal synthesis of Sn_3O_4/reduced graphene oxide (rGO) for excellent hydrogen generation under solar light.[24] To the best of our knowledge, very limited reports are available on Sn_3O_4/graphene composites for hydrogen generation under solar light.

Herein, we report an Sn_3O_4/graphene nanoheterostructure prepared by a facile hydrothermal route. Structural, optical and morphological studies of the Sn_3O_4/graphene composites were performed and are discussed. The resulting triclinic Sn_3O_4 has been demonstrated as a solar light-active photocatalyst for photocatalytic hydrogen generation under solar light. This work shows that the formation of a heterostructure between Sn_3O_4 nanoflakes and graphene extends the absorption into the visible region, and the nanocrystalline nature enhances hydrogen generation from H_2O and H_2S.

2. Experimental section

Stannous chloride ($SnCl_2 \cdot 2H_2O$, 99%, Fisher Scientific), 0.4 g of sodium hydroxide (NaOH, 99% SD Fine-Chem Ltd, India), and graphene used for the preparation of the catalysts were of analytical grade (SD Fine-Chem) and used without further purification.

2.1 Synthesis of Sn_3O_4/graphene

In a typical synthesis, the reagents were dissolved in distilled water. The detailed synthesis process was as follows. Stannous chloride (0.1 M, $SnCl_2 \cdot 2H_2O$, 99%, Fisher Scientific) and sodium hydroxide (1 M, NaOH, 99% SD Fine-Chem) were dissolved in 100 mL of distilled water and stirred for 20 min. The white solution was then transferred to a 120 mL Teflon autoclave and kept at 150 °C for 24 h. After washing several times with distilled water and, finally, with absolute ethanol, the faint yellow powder was obtained. This pure Sn_3O_4 sample was marked as Sng-0. For the preparation of Sn_3O_4/graphene nanostructures, the addition of graphene oxide (GO) (graphene oxide (10%) used as received) was performed *in situ* at different wt%, namely, 1, 2, 3, and 4 wt%, and the resultant products were labeled as Sng-1, Sng-2, Sng-3, and Sng-4, respectively.

2.2 Photocatalytic study

2.2.1 Photocatalytic hydrogen generation from water.
The photochemical reaction was carried in a 70 mL total volume, airtight cylindrical quartz reactor with a cooling jacket for water circulation. All the reactions were carried out at ambient conditions under natural sunlight on sunny days (March to May) between 10 am and 3 pm at Pune, Maharashtra State, India. The intensity of the solar light was measured by using a digital lux meter. The measured average intensity of solar light reaching the surface of the earth was 145 000 lux. In a typical photocatalytic experiment, 15 mg of the photocatalyst was dispersed in 25 mL total volume containing 20% methanol (v/v) in an aqueous solution. The 45 mL of free space of the photoreactor was made airtight with a rubber septum, followed by ultrasonication for 5 min for uniform dispersion of the catalyst. The solution mixture was then purged with ultra-high purity nitrogen gas (UHP 99.999%) to remove all the gases in the headspace of the reactor and dissolved oxygen from the reaction mixture. Before and after irradiation with solar light, the gas in the free space of the reactor was analyzed using gas chromatography (GC). The generated gas was analyzed immediately using GC with a specific time interval.

2.2.2 Photocatalytic hydrogen generation from H_2S.
The hydrogen generation was performed in a cylindrical quartz photochemical thermostatic reactor by introducing 0.5 g of Sn_3O_4/graphene. The reactor was filled with 700 mL of 0.5 M aqueous KOH and purged with argon for 30 min. Hydrogen sulfide was bubbled through the solution for 1 h at a rate of 2.5 mL min^{-1} at 299 K. Sn_3O_4/graphene photocatalyst was introduced as a suspension into a cylindrical quartz reactor and irradiated with sunlight with constant stirring with

a continuous flow of H_2S (2.5 mL min^{-1}). The excess H_2S was trapped in a 10% NaOH solution. The amount of H_2 gas evolved was measured using a graduated gas burette and analyzed using a gas chromatograph equipped with a thermal conductivity detector (TCD) and Porapak-Q packed column with N_2 as carrier gas.

2.3 Sample characterization

The phase formation and crystallite size of all synthesized samples were estimated via X-ray diffraction (XRD-D8, Advance, Bruker-AXS) with Ni-filtered Cu-Kα radiation ($\lambda = 1.5418$ Å). Optical properties of the bare and Au-loaded samples were studied by UV-visible-diffuse reflectance spectrometry (DRS) (UV 2600 spectrometer, Lambda-950, PerkinElmer) in the spectral range 200–800 nm. The surface morphology was characterized using field emission scanning electron microscopy (FESEM; Hitachi, S-4800 II) and field emission transmission electron microscopy (FETEM; JEM-2000 FS). Image processing and interplanar distance (d) evaluations were performed with the help of micrograph Gatan software. Surface characterization of all Sn_3O_4/graphene samples was carried out using X-ray photoelectron spectroscopy (XPS, ESCA-3000, VG Scientific Ltd) at a pressure > 1×10^{-9} torr. The general scan, C 1s, Sn 3d, and O 1s core-level spectra were recorded with non-monochromatized Mg-Kα radiation (photon energy 1253.6 eV). Baseline correction and peak fitting for all the samples was performed using the software package XPS peak-41. The core-level binding energies were aligned with respect to the C 1s binding energy of 285 eV. The collected gas sample was analyzed using a GC system (Shimadzu GC-2014) with a Portapak-Q packed column coupled with a TCD detector and UHP N_2 as carrier gas.

3. Results and discussion

3.1 Structural study

The Sn_3O_4 and Sn_3O_4/graphene composites were prepared by a facile one-step solvothermal method at 150 °C. The phase purity and crystallinity of the as-synthesized materials were determined by the X-ray diffraction patterns shown in Fig. 1(a). The diffraction peaks at 2θ values of 23.9°, 26.5°, 32.1°, 37.03°, 49.7°, and 51.56° correspond to the (1 0 1), (1 1 1), (2 1 0), (1 3 0), (3 1 1), and (1 3 2) lattice planes of triclinic Sn_3O_4 (JCPDS no. 16-0737) with lattice constants $a = 4.85$ Å, $b = 5.87$ Å and $c = 8.20$ Å, respectively.[25] It can be seen that there are no diffraction peaks of impurity phases, indicating the successful formation of Sn_3O_4. However, no diffraction peaks of graphene were observed in the XRD analysis, which may be due to the low concentration of graphene in the Sn_3O_4/graphene composites.

The presence of graphene was analyzed using a Raman study. Furthermore, structural features and chemical bonding between Sn_3O_4 and graphene were also investigated by Raman spectroscopy. The Raman spectra for pure Sn_3O_4 and Sn_3O_4/graphene are shown in Fig. 1(b). The high crystalline nature of the sample is evidenced by two sharp symmetric peaks observed at wavenumbers 120 and 167.8 cm^{-1}, due to the Sn–Sn

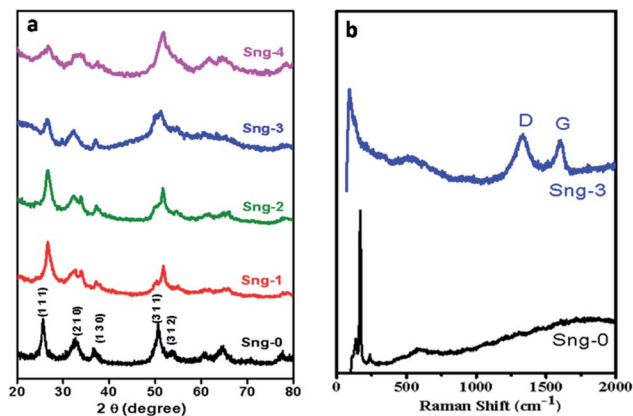Fig. 1 (a) XRD patterns of pure Sn_3O_4 (Sng-0), 1% graphene/Sn_3O_4 (Sng-1), 2% graphene/Sn_3O_4 (Sng-2), 3% graphene/Sn_3O_4 (Sng-3) and 4% graphene/Sn_3O_4 (Sng-4). (b) Raman shifts of pure Sn_3O_4 (Sng-0) and 3% graphene/Sn_3O_4 (Sng-3).

stretching vibration and phonon modes detected in the triclinic Sn_3O_4 structure.[26] The strong peak observed at a wavenumber of 630 cm^{-1} is ascribed to the Sn–O stretching vibration. Furthermore, Fig. 1(b) shows a peak positioned at 632 cm^{-1} for Sn–O, and two additional strong peaks are observed at 1348 and 1600 cm^{-1}, derived from the D and G bands of graphene.[27,28] Thus, the Raman study gives additional support to the existence of the triclinic Sn_3O_4/graphene structure suggested by the XRD study.

3.2 FESEM study

The morphological features of the as-prepared Sn_3O_4 and Sn_3O_4/graphene composites were studied using FESEM, as shown in Fig. 2. The FESEM images show spherical micro balls of pure Sn_3O_4. These micro balls are self-assembled with each other. The high-magnification FESEM images of Sn_3O_4/graphene (Fig. 2(c and d)) show Sn_3O_4 flakes of 15 nm thickness,
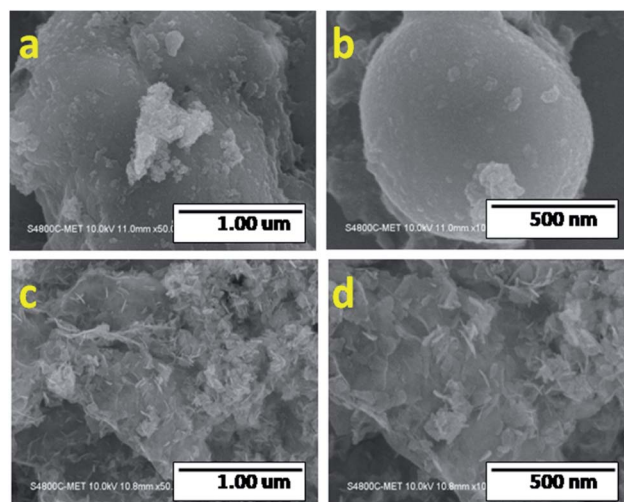

Fig. 2 FESEM images of pure Sn_3O_4 (a and b) and Sn_3O_4/graphene (Sng-3) (c and d).

which are grown on the graphene sheets. The ultra-thin 2D nanoflakes of Sn_3O_4/graphene intercalate with each other and form an array-like structure.

3.3 FETEM study

FETEM analysis was performed to determine the coexistence of graphene and Sn_3O_4, as shown in Fig. 3. Fig. 3(a and b) shows that the Sn_3O_4/graphene particles are 3D nanostructures having parallel and horizontal thin nanoflakes. The selected area electron diffraction (SAED) image insets of Fig. 3(a and b) show the points in the diffraction image of the marked (1 1 1) plane, with the index the same as for the single crystalline triclinic Sn_3O_4. As shown in Fig. 3(c and d) the lattice fringe spacing values of 0.329 nm, matching with the HR-TEM image, were indexed to the (1 1 1) crystallographic plane of triclinic Sn_3O_4. In addition, in Fig. 3(d) the graphene sheets can be seen. Further elemental mapping and energy dispersive X-ray analysis (EDAX) support the presence of Sn, O and C. Fig. 3(e) shows the EDAX spectra in which the atomic percentage of Sn, O, and C in Sn_3O_4/graphene composites were observed to be 28.44, 30.26 and 41.30%, respectively (Table 1). The elemental mapping study from scanning transmission electron microscopy (STEM) shows the presence of Sn, O, C. From the STEM, it can also be concluded that graphene was homogeneously dispersed in the Sn_3O_4 crystal, which indicates the formation of nanoflakes of high quality.

In the preparation of Sn_3O_4 graphene, the reaction between precursor salt solutions and aqueous NaOH solution established the formation of $Sn_4(OH)_2Cl_6$ and $2Cl^-$ nuclei under hydrothermal conditions (Scheme 1). The $Sn_4(OH)_2Cl_6$ reacts

Table 1 Elemental composition of the Sng-3 sample

Element	Weight%	Atomic%
C (K)	11.39	41.30
O (K)	11.12	30.26
Sn (L)	77.50	28.44
Totals	**100.00**	

with NaOH at 150 °C under hydrothermal conditions and forms Sn^{2+} cations. Further, Sn^{2+} cations are adsorbed onto the surface of the graphene sheets by coulombic forces of attraction. Due to prolonged heating at 150 °C under hydrothermal conditions, oxidation occurs and the formation of SnO takes place. The oxidation increases the coordination number of the Sn atoms by altering the density of the samples. Moreover, *in situ* Sn_3O_4 nuclei grow in parallel on the surface of the graphene. During this process, graphene $(C_nH_n(OH)_n)$ is reduced and releases –H and –OH ions. After the formation of Sn_3O_4 these nanoparticles become sandwiched between the layers of the graphene sheets. The as-synthesized Sn_3O_4/graphene composites were used for photocatalytic hydrogen generation.[29–31]

The overall reaction is as follows.[32]

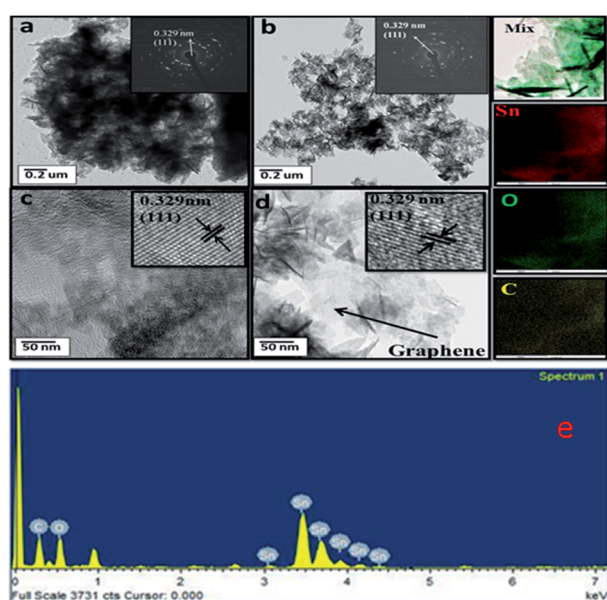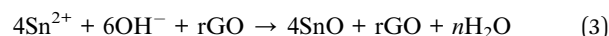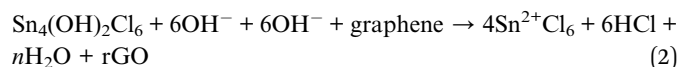$$4SnCl_2 + 2OH^- \rightarrow Sn_4(OH)_2Cl_6 + 2Cl^- \tag{1}$$

$$Sn_4(OH)_2Cl_6 + 6OH^- + 6OH^- + graphene \rightarrow 4Sn^{2+}Cl_6 + 6HCl + nH_2O + rGO \tag{2}$$

$$4Sn^{2+} + 6OH^- + rGO \rightarrow 4SnO + rGO + nH_2O \tag{3}$$

$$6SnO + 2O_2 + rGO \rightarrow 2Sn_3O_4/rGO \tag{4}$$

3.4 Optical properties

The light absorption properties of the as-synthesized materials were analyzed by UV-visible DRS spectroscopy. Fig. 4 shows the

Fig. 3 (a) FETEM images of pure Sn_3O_4 (a and c) and Sn_3O_4/graphene (Sng-3) (b and d) at low and high magnification and the corresponding SAED patterns, and EDAX of Sng-3. (e) STEM image of Sng-3 (3%) and EDS mapping: color map of mixture, Sn, O and C. Table 1 shows the elemental composition of the Sng-3 sample.
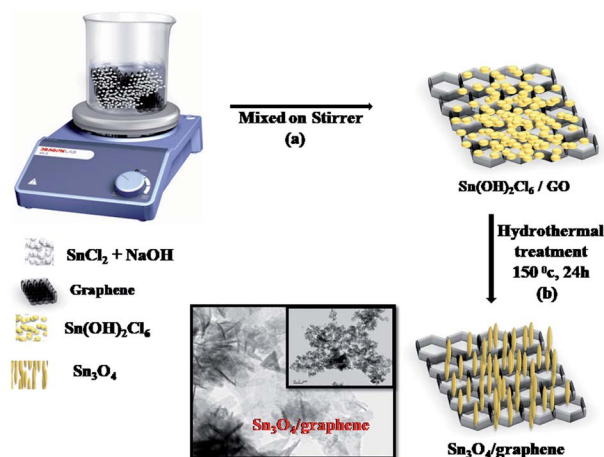
Scheme 1 Schematic representation of the formation mechanism of the Sn_3O_4/graphene nanostructure.

UV-DRS spectra of pristine Sn_3O_4 and Sn_3O_4/graphene composites. The pure Sn_3O_4 shows absorption at a wavelength of 430 nm. After incorporation of graphene the absorption edge is slightly extended to the visible region. Furthermore, a definite color change is observed, from pure yellow Sn_3O_4 to French grey for all the composites, after incorporation of graphene. The linear increase in absorption for the composites at a higher wavelength (>430 nm) is attributed to the intrinsic black-colored graphene. The band gap for Sn_3O_4 was calculated as 2.9 eV, *i.e.* absorption at 430 nm, which is further extended to the visible region due to graphene in the Sn_3O_4/graphene nanoheterostructure, which was calculated to be 2.5 eV, *i.e.* absorption at 490 nm.[32] This is attributed to the strong electronic interaction between graphene and Sn_3O_4, similar to that in TiO_2/graphene composites.[33] The main purpose of graphene is to increase the effective charge separation so that more efficient utilization of light can be obtained. Overall, the UV study showed that the introduction of graphene engineers the energy band structure of Sn_3O_4/graphene composites by interfacial interaction.

A photoluminescence (PL) study was employed to investigate recombination, trapping, migration, and transfer of charge carriers under visible light irradiation.

Fig. 5 shows the PL spectra of the as-synthesized pure Sn_3O_4 and the Sn_3O_4-decorated graphene nanoheterostructures. As can be seen from Fig. 5, the strong emission peak located at 510 nm is attributed to the intrinsic luminescence of Sn_3O_4.[34] Furthermore, it was observed that pure Sn_3O_4 and 1%, 2%, and 4% graphene showed lower PL intensity compared with the 3% graphene-decorated Sn_3O_4, but the main emission peak of the materials did not change significantly. The lowered PL intensity of graphene/Sn_3O_4 in comparison with Sn_3O_4 is ascribed to the photogenerated electrons from Sn_3O_4 being transferred into the carbon atoms of graphene, and therefore rapid charge recombination in the Sng-3 sample causes this to be reduced.[35] In addition, the Sng-3 sample was more active for surface oxygen
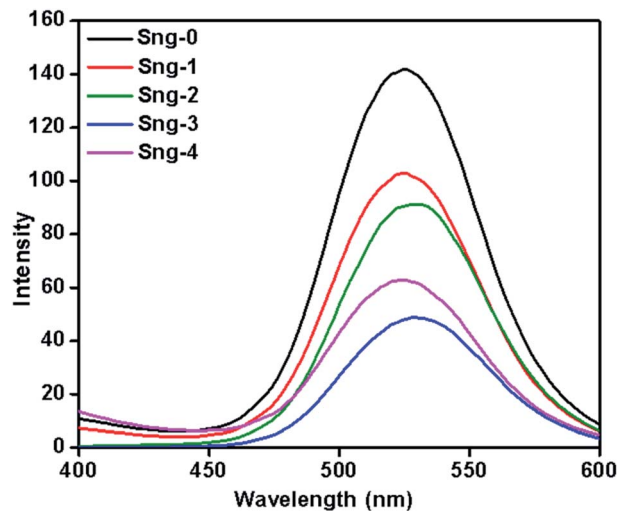

Fig. 5 PL spectra of pure Sn_3O_4 (Sng-0), 1% graphene/Sn_3O_4 (Sng-1), 2% graphene/Sn_3O_4 (Sng-2), 3% graphene/Sn_3O_4 (Sng-3) and 4% graphene/Sn_3O_4 (Sng-4).

vacancies and defects. At the same time, decoration of Sn_3O_4 on graphene is comparatively uniform, which might be helpful for fast electron transport. However, in the case of Sng-4, due to the high percentage of graphene, there is shielding of surface oxygen vacancies. Overall, the optimum concentration of graphene provides more charge carrier separation.

3.5 XPS study

The Sn_3O_4 and Sn_3O_4/graphene composites were analyzed by XPS spectra in a contrast manner to further confirm successful formation of the Sn_3O_4/graphene nanoheterostructures and to determine the elemental composition and valence states of Sn, O, and C. The Sn 3d, O 1s, and C 1s high-resolution XPS spectra provide more detailed information on the chemical state of these elements and are shown in Fig. 6(a–d).

Fig. 6(a) shows the doublet spectra for Sn 3d, split into $3d_{5/2}$ and $3d_{3/2}$ states at binding energies of 486.5, 495 and 487, 495.4 eV, for the Sng-0 and Sng-3 samples, respectively.[36] The slight shift in binding energy suggests that charge transfer takes place between the Sn_3O_4/graphene composites. The peaks located at binding energies 531 and 531.6 for O 1s are ascribed to the lattice oxygen and oxygen bound to the tin atom (Sn–O–Sn) in the Sng-0 and Sng-3 samples, respectively.[37] The chemical state of Sn in Sn_3O_4 and Sn_3O_4/graphene is the same, which means the residual O in graphene does not affect the chemical state of the Sn. The above results clearly show that the as-synthesized samples have a high oxygen vacancy. Furthermore, Fig. 6(d) shows that the C 1s spectrum of sample Sng-3 is split into four different peaks, at binding energies of 284.4, 285.14, 286.13, and 289.1 eV, which are due to C–C/C=C, C–O, C=O, and O–C=O bonds, respectively.[38,39]

The above discussion indicates that Sn_3O_4 and Sn_3O_4/graphene have the same binding energies except for the peak intensity of C 1s located in the Sn_3O_4/graphene composites, which introduces the strength of the Sng-3 sample. From the
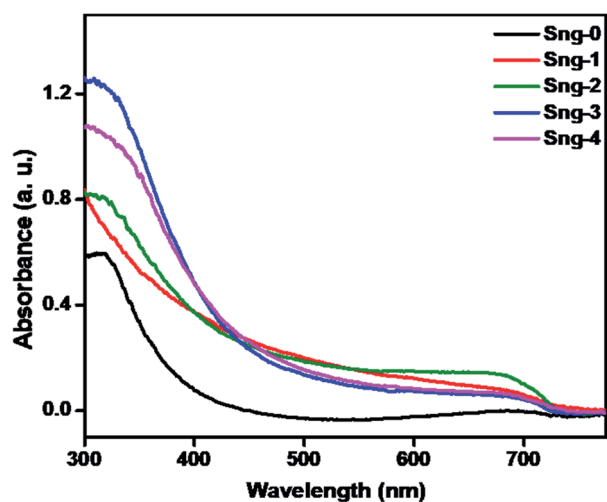

Fig. 4 UV-DRS spectra of pure Sn_3O_4 (Sng-0), 1% graphene/Sn_3O_4 (Sng-1), 2% graphene/Sn_3O_4 (Sng-2), 3% graphene/Sn_3O_4 (Sng-3) and 4% graphene/Sn_3O_4 (Sng-4).
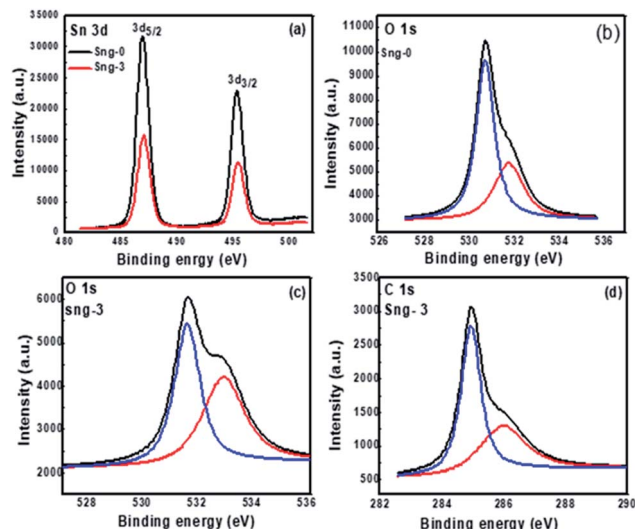
Fig. 6 XPS spectra of the as-prepared Sn_3O_4/graphene nano-structure: (a) Sn 3d, (b) O 1s (Sng-0), (c) O 1s (Sng-3), and (d) C 1s (Sng-3) samples.

above results, it is clear that Sn_3O_4 nanoparticles are distributed uniformly on the surface of the graphene sheets. Overall, the FETEM and UV-DRS results suggest that Sn_3O_4 was hybridized with graphene by successful formation of nanocomposites, providing synergistic interaction between Sn_3O_4 and graphene.

3.6 Photocatalytic study

3.6.1 Photocatalytic H_2 evolution from H_2O splitting. The photocatalytic hydrogen generation activities of the as-synthesized Sn_3O_4 and Sn_3O_4/graphene composites were studied under irradiation with natural sunlight. Fig. 7 shows the graph of the hydrogen evolution rate from water as a function of irradiation time. As shown in Fig. 7, the amount of
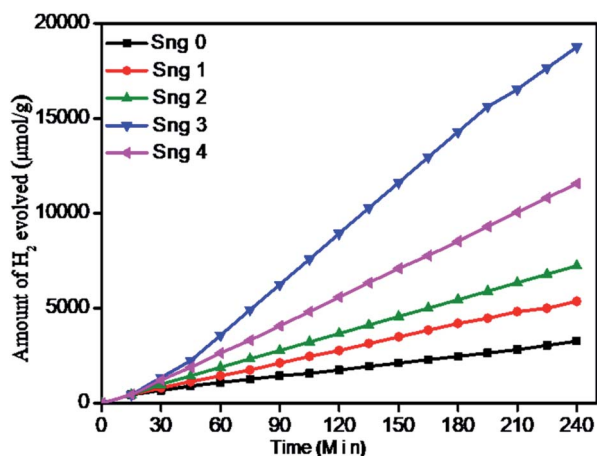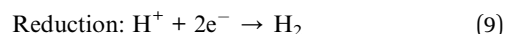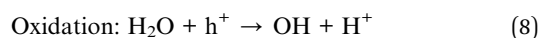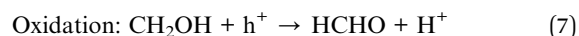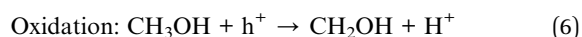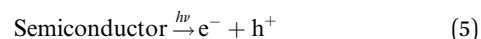

Fig. 7 Photocatalytic hydrogen production from water-splitting reaction using pure Sn_3O_4 (Sng-0), 1% graphene/Sn_3O_4 (Sng-1), 2% graphene/Sn_3O_4 (Sng-2), 3% graphene/Sn_3O_4 (Sng-3) and 4% graphene/Sn_3O_4 (Sng-4) samples.

hydrogen increases linearly with irradiation time for 4 h, for both Sn_3O_4 and Sn_3O_4/graphene composites.

The pure Sn_3O_4 nanoflakes show a hydrogen evolution rate of 815 $\mu mol\ h^{-1}\ g^{-1}$, whereas the Sn_3O_4/graphene composite shows a much higher rate of 4687 $\mu mol\ h^{-1}\ g^{-1}$, which is 5.7 times higher than that of pure Sn_3O_4 for a water-splitting reaction. Previously, J. Tang et al.[40] reported that methanol suppresses oxygen (O_2) evolution through the formation of free radicals, and also reduces charge carrier recombination by reacting irreversibly with photogenerated holes, which results in higher hydrogen yield. The basic photocatalytic mechanism was discussed in our previous study.[41] The surface of semi-conducting materials, when exposed to visible light equal to or greater than the band gap energy, generates electrons in the conductance band (CB) and holes in the valence band (VB) by excitation from the VB to the CB. The holes from the VB oxidize methanol and produce radicals as well as protons (H^+). The electrons from the CB reduce H^+ ions to form molecular hydrogen.[16] The generation of electron–hole pairs into semi-conductors and their migration on the reaction surface with aqueous methanol for water splitting is described as follows.

$$Semiconductor \xrightarrow{h\nu} e^- + h^+ \tag{5}$$

$$Oxidation:\ CH_3OH + h^+ \rightarrow CH_2OH + H^+ \tag{6}$$

$$Oxidation:\ CH_2OH + h^+ \rightarrow HCHO + H^+ \tag{7}$$

$$Oxidation:\ H_2O + h^+ \rightarrow OH + H^+ \tag{8}$$

$$Reduction:\ H^+ + 2e^- \rightarrow H_2 \tag{9}$$

3.6.2 Photocatalytic H_2 evolution from H_2S splitting. Over the last few years, graphene has been extensively studied as a supporting material for metal oxide/sulfide semiconductors, due to its unique electronic properties with large specific surface area, transparency, and excellent strength.[42,43] It is well known that graphene alone cannot produce hydrogen/oxygen under natural sunlight or generate electrons and holes, but graphene captures electrons and reduces the charge carrier recombination rate. However, composites of graphene with oxides/sulfides or nanoparticle-decorated graphene produce an excellent hydrogen generation rate. In the presence of dopant, cocatalyst, or the formation of defects in GO, photocatalytic hydrogen generation improves. Pristine Sn_3O_4 is a visible light-active catalyst, but rapid charge recombination and poor stability do not give significant hydrogen generation. Yu et al.[24] reported that Sn_3O_4 and its graphene composites showed enhanced H_2 generation under sunlight.

Fig. 8 shows the plot of H_2 generation against time from H_2S with Sn_3O_4/graphene composites. The linearity of the graph shows a steady hydrogen generation rate using sunlight. The maximum hydrogen generation for the water-splitting reaction, *i.e.* 4687 $\mu mol\ h^{-1}\ g^{-1}$, with a quantum efficiency of 3%, was attained using the Sn_3O_4/graphene (Sng-3) sample, whereas samples Sng-0, Sng-1, Sng-2, and Sng-4 show a rate of 815, 1384,

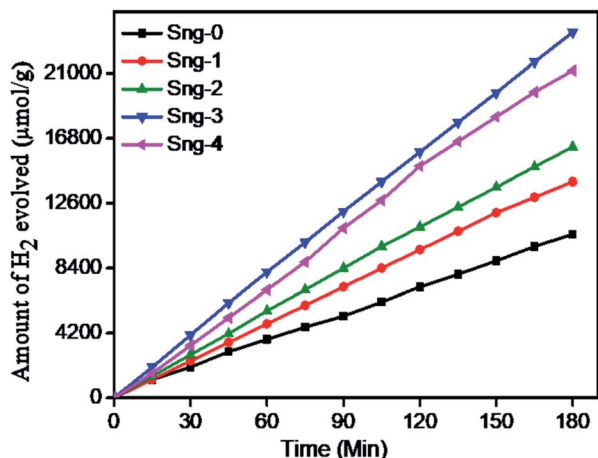Fig. 8 Photocatalytic hydrogen production from H_2S splitting reaction using pure Sn_3O_4 (Sng-0), 1% graphene/Sn_3O_4 (Sng-1), 2% graphene/Sn_3O_4 (Sng-2), 3% graphene/Sn_3O_4 (Sng-3), and 4% graphene/Sn_3O_4 (Sng-4).

$$H_2S + OH^- \leftrightarrow HS^- + H_2O \qquad (10)$$

$$H_2S + OH^- \leftrightarrow S^{2-} + H_2O \qquad (11)$$

$$\text{Photocatalyst} \rightarrow e_{CB}^- + h_{VB}^+ \qquad (12)$$

$$2S^{2-} + 2h_{VB}^+ \rightarrow S_2^{2-} \qquad (13)$$

$$2HS^- + 2h_{VB}^+ \rightarrow S_2^{2-} + 2H^+ \qquad (14)$$

$$2H^+ + 2e_{CB}^- \rightarrow H_2 \qquad (15)$$

1808, and 2890 µmol h^{-1} g^{-1} (Table 2). Considering the good photocatalytic performance of Sn_3O_4/graphene composites, we explored the evolution of H_2 from splitting of waste H_2S using the Sn_3O_4/graphene photocatalyst under visible light irradiation. For H_2S splitting, the highest hydrogen evolution was obtained with sample Sng-3, *i.e.* 7887 µmol h^{-1} g^{-1}, and for Sng-0, Sng-1, Sng-2, and Sng-4 the rates of hydrogen evolution were 3530, 4663, 5409, and 7061 µmol h^{-1} g^{-1}, respectively (Table 2). A similar trend was observed for both H_2O and H_2S splitting reactions, but the rate of hydrogen evolution for the H_2S splitting reaction is higher compared with that for H_2O and this is due to the lower ΔG value (33 kJ mol^{-1}) for the reaction. The detailed mechanism of H_2S splitting has already been discussed in our previous work.[44–46]

The mechanism of evolution of hydrogen gas *via* H_2S splitting was discussed in our previous article in detail.[36] In 0.5 M KOH solutions, the weak diprotic acid, H_2S, dissociates and maintains equilibrium with hydrogen disulfide (HS$^-$) ions. The Sn_3O_4/graphene semiconductors absorb light and generate electron–hole (e$^-$/h$^+$) pairs. The valence band hole (h$_{VB}^+$) is photogenerated after band gap excitation of the Sn_3O_4/graphene powder oxidizes the HS$^-$ ion to the disulfide ion (S$_2^{2-}$), liberating a proton from the HS$^-$ ion. The conduction band electron (e$_{CB}^-$) from the Sn_3O_4/graphene photocatalyst reduces the protons to produce molecular hydrogen.[37]
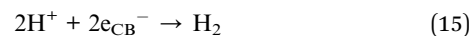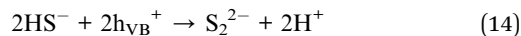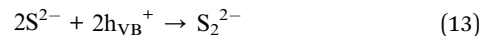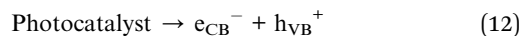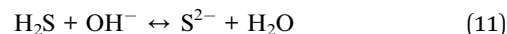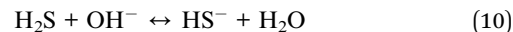
According to the literature, graphene is an electron acceptor owing to its π–π interactions and good electrical junctions due to its 2D planar structure. Here, 2D planar graphene is wrapped up in the Sn_3O_4 nanoflakes and can capture electrons and reduce charge carrier recombination. More electrons are available in Sn_3O_4/graphene for photoreduction of water, resulting in enhanced photocatalytic activity. Previously, Upadhyay *et al.*[47] reported that the interfacial interaction depends on the synthesis method, with the *in situ* growth approach being more attractive and efficient than other methods. The optimized quantity of graphene plays a crucial role in obtaining enhanced catalytic activity using Sn_3O_4/graphene composites. As discussed earlier, the maximum hydrogen generation, *i.e.* 4687 µmol h^{-1} g^{-1}, was obtained using the Sng-3 sample for H_2O splitting, and 7887 µmol h^{-1} g^{-1} was obtained for H_2S splitting. The improved photocatalytic activity can be ascribed to the following. (1) The pristine Sn_3O_4 has a sufficient response towards sunlight but the formation of composites with Sn_3O_4 supports enhanced photocatalytic activity. (2) The electrons are transferred from carbon atoms of graphene, *i.e.* the flat structure of graphene can transfer electrons freely, as well as from outer graphene sheets to inner sheets, and therefore the charge carrier recombination rate is reduced. (3) The strong hybridization interaction between graphene and Sn_3O_4 (by the formation of C–O bonds) can reduce activation of the surface oxygen atom of Sn_3O_4 and leads to excellent stability. Furthermore, due to hybridization, the absorption is extended towards longer wavelengths, thus there is enhanced absorption in the visible region and so utilizing maximum sunlight for the photocatalytic process. (4) These advanced 2D materials mean that hybridization of Sn_3O_4 and GO-derived graphene can effectively transfer the merits of Sn_3O_4 and GO to obtain excellent photocatalytic activity. (5) More significantly, the unique features of Sn_3O_4/graphene composites provide a large surface area,

Table 2 Photocatalytic hydrogen evolution *via* water and H_2S splitting

Sr. no.	Sample code	H_2 evolution rate from water (µmol h^{-1} g^{-1})	H_2 evolution rate from H_2S (µmol h^{-1} g^{-1})
1	Sng-0	815	3530
2	Sng-1	1384	4663
3	Sng-2	1808	5409
4	Sng-3	4687	7887
5	Sng-4	2890	7061

smaller particle diameter, and faster transfer of charge carriers from the inside to the surface, which hampers the probability of charge recombination and also allows more active adsorption sites for a redox reaction to start (Scheme 2). Furthermore, the presence of graphene resists the growth of Sn_3O_4, therefore the optimum quantity of graphene (3%) is dispersed on a large surface of graphene. These combined factors are responsible for the enhanced hydrogen generation. However, it was also seen that increase in the concentration of graphene in Sn_3O_4 reduces the photocatalytic activity for the Sng-4 Sn_3O_4/graphene composite. Previously, Zhang et al.[48] reported that a higher percentage of graphene causes a shielding effect, which decreases active sites on the photocatalyst surface resulting in high charge carrier recombination rates, i.e. at higher absorption light scatters through excess graphene in the photosystem, resulting in lower excitation efficiency of Sn_3O_4. In addition, from the above study, it is concluded that the Sn_3O_4/graphene provides more electrons and holes to the surface of the photocatalyst and is tracked into the graphene sheets, reducing the recombination rate. The optimum quantity of graphene (3% graphene) loaded on Sn_3O_4 suppresses the recombination of photogenerated electrons and holes.

4. Conclusions

A series of Sn_3O_4/graphene composites have been successfully prepared by a simple one-step hydrothermal route. The morphological study shows the as-synthesized composites were a uniform size and the average diameter varies from one to several micrometers. The optical properties of Sn_3O_4/graphene show enhanced absorption in the visible region. The photocatalytic activity of the catalysts (Sn_3O_4/graphene) towards hydrogen generation, from water and H_2S under solar light, have been demonstrated. The Sn_3O_4/graphene composites exhibit higher photocatalytic activity compared with bare Sn_3O_4. The optimum quantity of graphene (3% graphene-decorated Sn_3O_4) shows an enhanced H_2 generation rate, namely 4687 µmol h^{-1} g^{-1}, for water splitting, and 7887 µmol h^{-1} g^{-1} for H_2S splitting, under natural sunlight. The enhanced photocatalytic activity could be ascribed to the extended absorbance via multiple reflections, and synergy between Sn_3O_4 and graphene reducing the charge carrier recombination efficiently. In addition, this work presents new insights for the development of graphene with oxide composite photocatalysts, and promotes their utilization for hydrogen energy generation.

Conflicts of interest

There are no conflicts to declare.

Acknowledgements

References

1 C. Xu, P. Ravi Anusuyadevi, C. Aymonier, R. Luque and S. Marre, Nanostructured Materials for Photocatalysis, Chem. Soc. Rev., 2019, 48, 3868–3902.

2 H. Zhou, Y. Qu, T. Zeid and X. Duan, Towards Highly Efficient Photocatalysts Using Semiconductor Nanoarchitectures, Energy Environ. Sci., 2012, 5, 6732–6743.

3 A. Fujishima and K. Honda, TiO_2 Photoelectrochemistry and Photocatalysis, Nature, 1972, 238, 37–38.

4 G. N. Shao, H. Kim and S. Imran, https://www.Sciencedirect.com/Science/Article/Abs/Pii/S092633731500346x, 2016.

5 M. Dhiman, A. Maity, A. Das, R. Belgamwar, B. Chalke, Y. Lee, K. Sim, J.-M. Nam and V. Polshettiwar, Plasmonic Colloidosomes of Black Gold for Solar Energy Harvesting and Hotspots Directed Catalysis for CO_2 to Fuel Conversion, Chem. Sci., 2019, 10, 6594–6603.

6 S. Sfaelou, L.-C. Pop, O. Monfort, V. Dracopoulos and P. Lianos, Mesoporous WO_3 Photoanodes for Hydrogen Production by Water Splitting and Photofuelcell Operation, Int. J. Hydrogen Energy, 2016, 41, 5902–5907.

7 Y. Wu, S. Zeng, Y. Dong, Y. Fu, H. Sun, S. Yin, X. Guo and W. Qin, Hydrogen Production from Methanol Aqueous Solution by $ZnO/Zn(OH)_2$ Macrostructure Photocatalysts, RSC Adv., 2018, 8, 11395–11402.

8 W. Hou and S. B. Cronin, A Review of Surface Plasmon Resonance-Enhanced Photocatalysis, Adv. Funct. Mater., 2013, 23, 1612–1619.

9 R. Acharya and K. Parida, A Review on TiO_2/g-C_3N_4 Visible-Light- Responsive Photocatalysts for Sustainable Energy
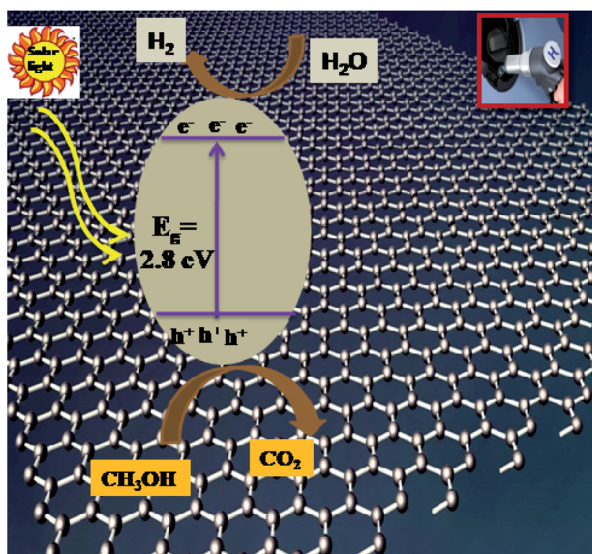
Scheme 2 Schematic representation of the photocatalytic mechanism of the Sn_3O_4/graphene nanostructure.

Generation and Environmental Remediation, *J. Environ. Chem. Eng.*, 2020, **8**, 103896.

10 M. A. Mahadadalkar, S. W. Gosavi and B. B. Kale, Interstitial Charge Transfer Pathways in a TiO₂/CdIn₂S₄ Heterojunction Photocatalyst for Direct Conversion of Sunlight into Fuel, *J. Mater. Chem. A*, 2018, **6**, 16064–16073.

11 F. E. Osterloh, Inorganic Materials as Catalysts for Photochemical Splitting of Water, *Chem. Mater.*, 2008, **20**, 35–54.

12 J. Zheng, H. Zhou, Y. Zou, R. Wang, Y. Lyu, S. P. Jiang and S. Wang, Efficiency and Stability of Narrow-Gap Semiconductor-Based Photoelectrodes, *Energy Environ. Sci.*, 2019, **12**, 2345–2374.

13 I. Staffell, D. Scamman, A. Velazquez Abad, P. Balcombe, P. E. Dodds, P. Ekins, N. Shah and K. R. Ward, The Role of Hydrogen and Fuel Cells in the Global Energy System, *Energy Environ. Sci.*, 2019, **12**, 463–491.

14 A. K. Kulkarni, R. P. Panmand, Y. A. Sethi, S. R. Kadam, S. P. Tekale, G. H. Baeg, A. V. Ghule and B. B. Kale, In Situ Preparation of N Doped Orthorhombic Nb₂O₅ Nanoplates/ rGO Composites for Photocatalytic Hydrogen Generation under Sunlight, *Int. J. Hydrogen Energy*, 2018, **43**, 19873–19884.

15 A. Kudo and Y. Miseki, Heterogeneous Photocatalyst Materials for Water Splitting, *Chem. Soc. Rev.*, 2009, **38**, 253–278.

16 X. Chen, S. Shen, L. Guo and S. S. Mao, Semiconductor-Based Photocatalytic Hydrogen Generation, *Chem. Rev.*, 2010, **110**, 6503–6570.

17 R. K. Chava, J. Y. Do and M. Kang, Enhanced Photoexcited Carrier Separation in CdS–SnS₂ Heteronanostructures: A New 1D–0D Visible-Light Photocatalytic System for the Hydrogen Evolution Reaction, *J. Mater. Chem. A*, 2019, **7**, 13614–13628.

18 D. Zeng, C. Yu, Q. Fan, J. Zeng, L. Wei, Z. Li, K. Yang and H. Ji, Theoretical and Experimental Research of Novel Fluorine Doped Hierarchical Sn₃O₄ Microspheres with Excellent Photocatalytic Performance for Removal of Cr(Vi) and Organic Pollutants, *Chem. Eng. J.*, 2020, **391**, 123607.

19 J. Hu, X. Li, X. Wang, Q. Li and F. Wang, Novel Hierarchical Sn₃O₄/BiOX (X= Cl, Br, I) p–n Heterostructures with Enhanced Photocatalytic Activity under Simulated Solar Light Irradiation, *Dalton Trans.*, 2019, **48**, 8937–8947.

20 G. Chen, S. Ji, Y. Sang, S. Chang, Y. Wang, P. Hao, J. Claverie, H. Liu and G. Yu, Synthesis of Scaly Sn₃O₄/TiO₂ Nanobelt Heterostructures for Enhanced UV-Visible Light Photocatalytic Activity, *Nanoscale*, 2015, **7**, 3117–3125.

21 A. Geim and K. Novoselov, *Nat. Mater.*, 2007, **6**(3), 183.

22 T.-F. Yeh, C.-Y. Teng, L.-C. Chen, S.-J. Chen and H. Teng, Graphene Oxide-Based Nanomaterials for Efficient Photoenergy Conversion, *J. Mater. Chem. A*, 2016, **4**, 2014–2048.

23 A. Bhirud, S. Sathaye, R. Waichal, C.-J. Park and B. Kale, In Situ Preparation of N–ZnO/Graphene Nanoheterostructure: Excellent Candidate as a Photocatalyst for Enhanced Solar Hydrogen Generation and High Performance

Supercapacitor Electrode, *J. Mater. Chem. A*, 2015, **3**, 17050–17063.

24 X. Yu, Z. Zhao, D. Sun, N. Ren, J. Yu, R. Yang and H. Liu, Microwave-Assisted Hydrothermal Synthesis of Sn₃O₄ Nanosheet/rGO Planar Heterostructure for Efficient Photocatalytic Hydrogen Generation, *Appl. Catal., B*, 2018, **227**, 470–476.

25 J. Wang, N. Umezawa and H. Hosono, Mixed Valence Tin Oxides as Novel Van Der Waals Materials: Theoretical Predictions and Potential Applications, *Adv. Energy Mater.*, 2016, **6**, 1501190.

26 F. Yin, Y. Li, W. Yue, S. Gao, C. Zhang and Z. Chen, Sn₃O₄/ rGO Heterostructure as a Material for Formaldehyde Gas Sensor with a Wide Detecting Range and Low Operating Temperature, *Sens. Actuators, B*, 2020, 127954.

27 X. Pan and Z. Yi, Graphene Oxide Regulated Tin Oxide Nanostructures: Engineering Composition, Morphology, Band Structure, and Photocatalytic Properties, *ACS Appl. Mater. Interfaces*, 2015, **7**, 27167–27175.

28 M.-Q. Yang, N. Zhang, M. Pagliaro and Y.-J. Xu, Artificial Photosynthesis over Graphene–Semiconductor Composites. Are We Getting Better?, *Chem. Soc. Rev.*, 2014, **43**, 8240–8254.

29 X. Yu, Z. Zhao, N. Ren, J. Liu, D. Sun, L. Ding and H. Liu, Top or Bottom, Assembling Modules Determine the Photocatalytic Property of the Sheetlike Nanostructured Hybrid Photocatalyst Composed with Sn₃O₄ and rGO (GOD), *ACS Sustainable Chem. Eng.*, 2018, **6**, 11775–11782.

30 M. Manikandan, T. Tanabe, P. Li, S. Ueda, G. V. Ramesh, R. Kodiyath, J. Wang, T. Hara, A. Dakshanamoorthy and S. Ishihara, Photocatalytic Water Splitting under Visible Light by Mixed-Valence Sn₃O₄, *ACS Appl. Mater. Interfaces*, 2014, **6**, 3790–3793.

31 J. J. De Yoreo and P. G. Vekilov, Principles of Crystal Nucleation and Growth, *Rev. Mineral. Geochem.*, 2003, **54**, 57–93.

32 C. Yu, D. Zeng, Q. Fan, K. Yang, J. Zeng, L. Wei, J. Yi and H. Ji, The Distinct Role of Boron Doping in Sn₃O₄ Microspheres for Synergistic Removal of Phenols and Cr(Vi) in Simulated Wastewater, *Environ. Sci.: Nano*, 2020, **7**, 286–303.

33 S. A. Khan, Z. Arshad, S. Shahid, I. Arshad, K. Rizwan, M. Sher and U. Fatima, Synthesis of TiO₂/Graphene Oxide Nanoheterostructure for Their Enhanced Photocatalytic Activity against Methylene Blue Dye and Ciprofloxacin, *Composites, Part B*, 2019, **175**, 107120.

34 S. Balgude, Y. Sethi, A. Gaikwad, B. Kale, D. Amalnerkar and P. Adhyapak, Unique N Doped Sn₃O₄ Nanosheets as an Efficient and Stable Photocatalyst for Hydrogen Generation under Sunlight, *Nanoscale*, 2020, **12**, 8502–8510.

35 C. Li, S. Yu, H. Dong, C. Liu, H. Wu, H. Che and G. Chen, Z-Scheme Mesoporous Photocatalyst Constructed by Modification of Sn₃O₄ Nanoclusters on g-C₃N₄ Nanosheets with Improved Photocatalytic Performance and Mechanism Insight, *Appl. Catal., B*, 2018, **238**, 284–293.

36 W. Xia, H. Wang, X. Zeng, J. Han, J. Zhu, M. Zhou and S. Wu, High-Efficiency Photocatalytic Activity of Type II SnO/Sn₃O₄ Heterostructures Via Interfacial Charge Transfer, *CrystEngComm*, 2014, **16**, 6841–6847.

37 A. W. Cook, P. Hrobárik, P. L. Damon, G. Wu and T. W. Hayton, A Ketimide-Stabilized Palladium Nanocluster with a Hexagonal Aromatic Pd7 Core, *Inorg. Chem.*, 2020, **59**, 1471–1480.

38 F. Meng, J. Li, S. K. Cushing, M. Zhi and N. Wu, Solar Hydrogen Generation by Nanoscale P–N Junction of P-Type Molybdenum Disulfide/N-Type Nitrogen-Doped Reduced Graphene Oxide, *J. Am. Chem. Soc.*, 2013, **135**, 10286–10289.

39 X. Chen, Y. Huang, T. Li, C. Wei, J. Yan and X. Feng, Self-Assembly of Novel Hierarchical Flowers-Like Sn_3O_4 Decorated on 2D Graphene Nanosheets Hybrid as High-Performance Anode Materials for Libs, *Appl. Surf. Sci.*, 2017, **405**, 13–19.

40 J. Tang, J. R. Durrant and D. R. Klug, Mechanism of Photocatalytic Water Splitting in TiO_2. Reaction of Water with Photoholes, Importance of Charge Carrier Dynamics, and Evidence for Four-Hole Chemistry, *J. Am. Chem. Soc.*, 2008, **130**, 13885–13891.

41 Y. A. Sethi, A. K. Kulkarni, S. K. Khore, R. P. Panmand, S. C. Kanade, S. W. Gosavi, M. V. Kulkarni and B. B. Kale, Plasmonic Ag Decorated $CdMoO_4$ as an Efficient Photocatalyst for Solar Hydrogen Production, *RSC Adv.*, 2019, **9**, 28525–28533.

42 G. Xie, K. Zhang, B. Guo, Q. Liu, L. Fang and J. R. Gong, Graphene-Based Materials for Hydrogen Generation from Light-Driven Water Splitting, *Adv. Mater.*, 2013, **25**, 3820–3839.

43 S. Balgude, Y. Sethi, B. Kale, D. Amalnerkar and P. Adhyapak, Sn_3O_4 Microballs as Highly Efficient Photocatalyst for Hydrogen Generation and Degradation of Phenol under natural sunlightIrradiation, *Mater. Chem. Phys.*, 2019, **221**, 493–500.

44 A. R. Gunjal, A. K. Kulkarni, U. V. Kawade, Y. A. Sethi, R. S. Sonawane, J. Ook-Baeg, A. V. Nagawade and B. B. Kale, A Hierarchical $SnS@ZnIn_2S_4$ Marigold Flower-Like 2D Nano-Heterostructure as an Efficient Photocatalyst for Sunlight-Driven Hydrogen Generation, *Nanoscale Adv.*, 2020, **2**, 2577–2586.

45 B. B. Kale, J.-O. Baeg, S. M. Lee, H. Chang, S.-J. Moon and C. W. Lee, $CdIn_2S_4$ Nanotubes and "Marigold" Nanostructures: A Visible-Light Photocatalyst, *Adv. Funct. Mater.*, 2006, **16**, 1349–1354.

46 A. G. De Crisci, A. Moniri and Y. Xu, Hydrogen from Hydrogen Sulfide: Towards a More Sustainable Hydrogen Economy, *Int. J. Hydrogen Energy*, 2019, **44**, 1299–1327.

47 R. K. Upadhyay, N. Soin and S. S. Roy, Role of Graphene/Metal Oxide Composites as Photocatalysts, Adsorbents and Disinfectants in Water Treatment: A Review, *RSC Adv.*, 2014, **4**, 3823–3851.

48 Y. Liang, X. He, L. Chen and Y. Zhang, Preparation and Characterization of TiO_2–Graphene@Fe_3O_4 Magnetic Composite and Its Application in the Removal of Trace Amounts of Microcystin-Lr, *RSC Adv.*, 2014, **4**, 56883–56891.